Review

Diffusion Weighted Imaging in Neuro-Oncology: Diagnosis, Post-Treatment Changes, and Advanced Sequences—An Updated Review

Andrea Romano [1], Serena Palizzi [1], Allegra Romano [1], Giulia Moltoni [1,*], Alberto Di Napoli [1,2], Francesca Maccioni [3] and Alessandro Bozzao [1]

1   NESMOS Department, U.O.C. Neuroradiology, "Sant'Andrea" University Hospital, 00189 Rome, Italy
2   IRCCS Fondazione Santa Lucia, 00179 Rome, Italy
3   Department of Radiology, Sapienza University of Rome, Viale Regina Elena 324, 00161 Rome, Italy
*   Correspondence: giulia.moltoni@uniroma1.it; Tel.: +39-3347906958

Simple Summary: Differential diagnosis among primary and secondary central nervous system tumors, the assessment of tumoral therapy response, the correlation between imaging and prognosis, and biomolecular findings remain the main diagnostic challenges in the neuro-oncology imaging field. In the literature, novel, sophisticated MRI sequences and applications of artificial intelligence are frequently researched with this goal in mind; anyway, some of these tools are still not applicable in clinical practice. On the contrary, Diffusion Weighted Imaging (DWI) is a sequence commonly used in everyday clinical practice that can give information in terms of tumor grading, differential diagnosis, molecular profile, and response to therapy.

Abstract: DWI is an imaging technique commonly used for the assessment of acute ischemia, inflammatory disorders, and CNS neoplasia. It has several benefits since it is a quick, easily replicable sequence that is widely used on many standard scanners. In addition to its normal clinical purpose, DWI offers crucial functional and physiological information regarding brain neoplasia and the surrounding milieu. A narrative review of the literature was conducted based on the PubMed database with the purpose of investigating the potential role of DWI in the neuro-oncology field. A total of 179 articles were included in the study.

Keywords: diffusion-weighted imaging; magnetic resonance imaging; tumors

1. Introduction

Diffusion-weighted imaging (DWI) is a magnetic resonance imaging (MRI) sequence commonly used in neuroradiology for the assessment of acute ischemia, inflammatory diseases, and central nervous system (CNS) neoplasia [1–3].

It has several advantages, as it is a fast, easily reproducible, and extensively studied sequence in neuro-oncology, and it is widely available on many standard scanners, including those in non-academic centers [4,5].

In addition to being a simple instrument for everyday use, DWI can also offer functional and ultrastructural data, particularly when discussing tumor cellularity and the microenvironment through the measurement of water mobility. In fact, it yields an imaging biomarker for pathological tissue changes like cellularity increase or anomalies in the extracellular space by the assessment of water mobility [6–8].

Moreover, advanced diffusion-related sequences such as Diffusion Tensor Imaging (DTI) and Diffusion Kurtosis Imaging (DKI) are even playing a more important role than DWI in the neuro-oncology field.

Finally, multi-shell diffusion MRI allows for characterizing the water diffusion signal behavior by analyzing the data using multi-compartment diffusion models such as the

Neurite Orientation Dispersion and Density Imaging (NODDI) model. Thus, it can provide a more specific characterization of brain tissue microstructures than conventional single-shell diffusion tensor imaging.

2. Gliomas and Cellularity

Brain tumors may show various degrees of diffusion changes related to tumor cellularity and the nucleus-cytoplasmic ratio [9]. Water diffusion restriction secondary to tumor high-cellularity results in low Apparent Diffusion Coefficient (ADC) values, which are useful for differentiating tumor type and grade [6,10,11]. The minimal ADC value has been proposed as one of the various parameters to use as a predictive tool in patients with malignant supratentorial astrocytomas [12–18]. For instance, Moon et al. [12], Yamasaki et al. [13], and Murakami et al. [14] showed an inverse correlation between the mean ADC value and tumor grade in astrocytic tumors. Generally, higher-grade tumors typically have lower ADC values (Figure 1A–H). Due to their variable cellularity and grade, astrocytomas exhibit heterogeneous diffusion signals, with most cellular areas generally exhibiting restricted diffusion [9]. For instance, the degree of ADC hypointensity will often be higher in lymphoma than in glioma or metastases, reflecting the high cellular density in this neoplasm. The drop in ADC values for non-necrotic high-grade gliomas and metastases will be higher than for low-grade malignancies. High-grade tumor-associated edema reduces ADC sensitivity by raising the average ADC intensity [6,7]. ADC values alone or in combination with other MRI parameters, such as relative cerebral blood volume (rCBV), derived by dynamic susceptibility contrast-enhanced MR-perfusion (DSC), can accurately grade gliomas [19]. Indeed, Wang et al. recently reported a high accuracy of DWI/ADC to distinguish low-grade gliomas (grades I and II) from high-grade ones (grades III and IV) with an area under the curve (AUC) of 0.91; therefore, with this value being very high it reflects an excellent diagnostic performance of DWI in this field [9,20].
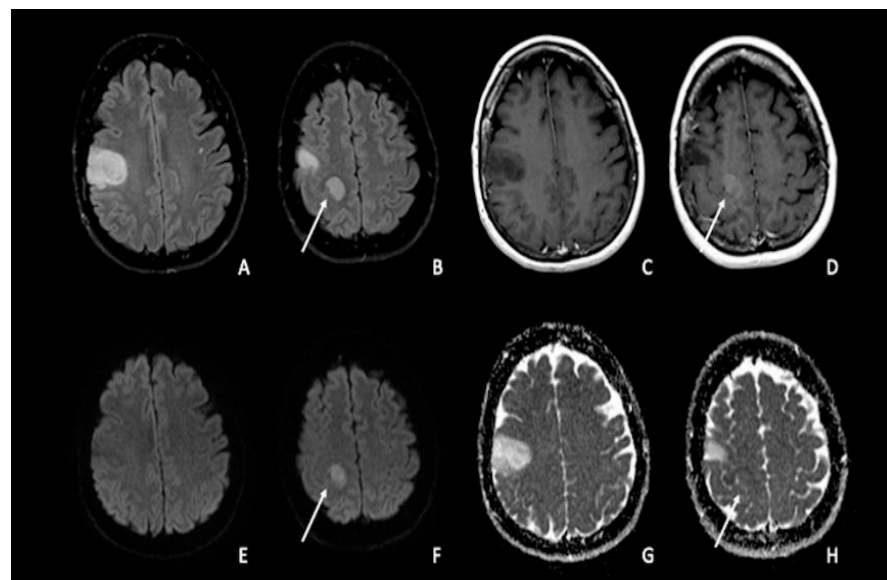

Figure 1. Double site of glioma infiltration in the right Rolandic frontal region: (**A**,**B**) Both lesions present similar hyperintensity on FLAIR images. The most cranial lesion (arrow) showed slight post-contrastographic enhancement (**D**) and restricted water diffusion on DWI (**F**), characterized by slightly low values on ADC map (**H**); this condition could be linked to an anaplastic aspect of the tumor, with restricted diffusion explained by an increase in tumor cellularity. The most caudal lesion did not show contrast enhancement, with a marked hypointense signal on post-contrastographic T1-weighted image (**C**); the same lesion presented no restricted diffusion with increased ADC values (**E**–**G**). FLAIR = fluid-attenuated inversion recovery; DWI = diffusion-weighted imaging; ADC: apparent diffusion coefficient.

In addition to standard DWI acquisition, more advanced models of quantitative DWI, such as DTI and DKI, have been created. These advanced sequences try to go beyond the theory that water diffusion occurs without boundaries via a uniform Gaussian distribution; indeed, it also depends on the configuration of intracellular organelles, cell membranes, and water compartments in cerebral tissues [6,21,22]. For instance, thanks to DKI, it is possible to quantify the deviation from a Gaussian distribution to produce a more accurate model [6,23,24]. The same result was reached by Abdalla et al. in a more recent expanded and updated meta-analysis, which found that DKI offers good diagnostic accuracy in differentiating high-grade from low-grade gliomas [6,25].

Finally, intravoxel incoherent motion (IVIM) and neurite orientation and dispersion imaging (NODDI), which make use of multiband imaging, are two promising advanced DTI approaches [6,26]. NODDI, in particular, measures the microstructure of dendrites and axons, revealing neuronal alterations, whereas IVIM may estimate tissue diffusivity and microcapillary perfusion [6].

3. Gliomas and Molecular Biology

When considering the glial line neoplasm, the 2016 World Health Organization (WHO) classification system has defined various groups of diffuse low-grade gliomas (LGGs) considering the isocitrate dehydrogenase (IDH) mutation and 1p/19q codeletion status [27,28]. The WHO classification of 2021 increased the importance of the molecular profile of brain tumors by categorizing adult-type diffuse glioma into three groups: IDH mutant with 1p/19q codeletion (Oligodendroglioma/IDH-mut codeleted LGGs), IDH mutant without codeletion (Astrocytoma/IDH-mut non-codeleted), and IDH wild type (Glioblastoma) [29]. The IDH gene plays a crucial role in metabolism, cellularity, and angiogenesis [30]. Recent research has shown that IDH mutant gliomas exhibit significantly greater survival and chemosensitivity than IDH wild-type glioblastomas [31,32]. When the IDH gene family is mutated, an oncometabolite called 2-hydroxyglutarate is produced, which inhibits tumor cell proliferation more than the wild type [33,34]. When compared to astrocytomas, oligodendrogliomas have a superior clinical outcome and treatment response [29,31,35–37]. As IDH mutant inhibitors become commercially available and might even be employed as neoadjuvant therapy, imaging biomarkers of IDH mutation would be a useful adjunct tool for clinical decision-making [38]. As a result, numerous research studies [33,39–65] investigated the imaging properties and/or high diagnostic performance of various MRI sequences for the prediction of IDH mutations in gliomas. According to several studies [41,48,56,60,62], IDH mutant glioma consistently displays higher mean ADC values on DWI than IDH wild-type glioblastoma [34]. It is still unclear how IDH-mutant and IDH wild-type gliomas differ from one another in terms of the ADC values; however, it could possibly be primarily related to tumor cellularity but also to the presence of cystic components, areas of necrosis, and interstitial water content [17,18,66]. While most IDH wild-type gliomas commonly present high-grade features such as necrosis and lower ADC mean values in solid sections, perhaps indicating more cellularity, most IDH-mutant gliomas show higher ADC mean values and MR imaging features consistent with a lower-grade nature [37] (Figure 2A–H). When considering oligodendrogliomas and the relationship between the 1p/19q codeletion status and ADC levels, the literature has shown contradictory findings [56,67–69]. According to Jenkinson et al., IDH-mut non-codeleted LGGs had much higher ADC values than IDH-mut-codeleted LGGs. Compared to IDH-mut non-codelated LGGs, the IDH-mut codeleted group may have fewer edematous areas and more cellulated areas, which could account for the lower ADC values [29,68]. Other diffusion-based sequences, such as DTI, DKI, and NODDI, have been successfully tested in predicting IDH status in gliomas, both with and without the use of artificial intelligence [70,71], with similar results between DTI and more advanced multi-shell methods [71,72]. Interestingly, mean diffusivity (MD) measures were increased in tumors not usually associated with high cellularity, probably reflecting changes in the extracellular volume that play a role in the diffusion signal [71]. Epidermal Growth Factor (EGFR) amplification is a

molecular biomarker that could allow glioblastoma IDH wild-type designation even in tumors that appear histologically lower grade [29]. Hence, its prediction through MRI could be of therapeutic and prognostic use. A recent pilot study found that EGFR-amplified tumors showed lower mean ADC values compared to EGFR-non-amplified tumors [73]. Future research could focus on other important molecular information in gliomas, such as CDKN2A/B deletion or combined whole chromosome 7 gain and whole chromosome 10 loss (+7/−10) mutations.
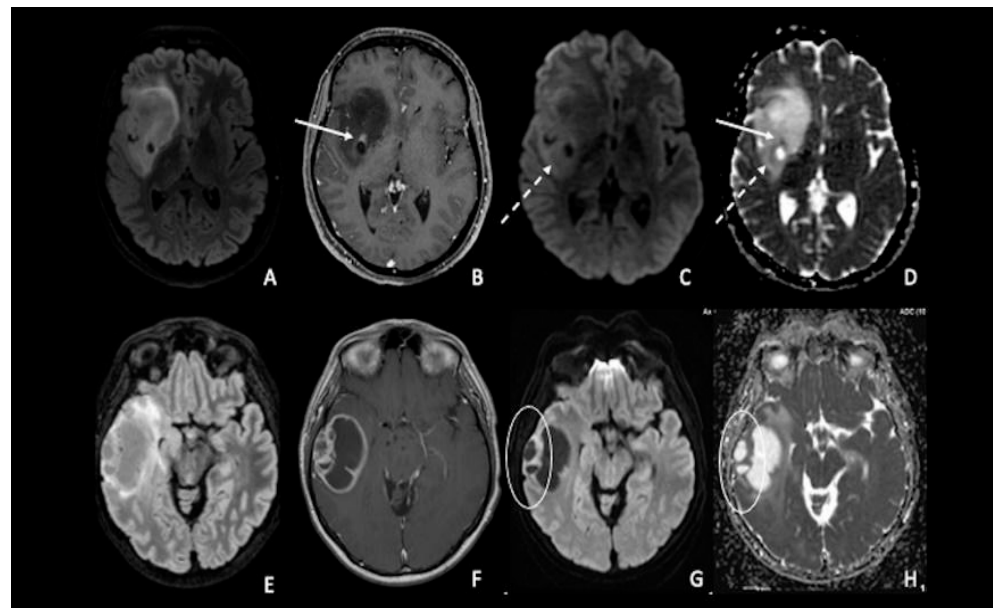

Figure 2. (**A**–**D**) IDH-1 mutated glioma in the right Sylvian region. The lesion is characterized by a heterogenous signal on FLAIR (**A**), with a small area of nodular enhancement on post-contrastographic T1 weighted images (arrow) (**B**); The site of pathological enhancement was in close proximity to an area of cystic-necrotic degeneration (dotted arrow) (**C**,**D**) and showed restricted diffusion on DWI confirmed by the ADC map (arrow); these findings were consistent with an anaplastic behavior of the tumor. (**E**–**H**) Right temporal lobe glioblastoma. The lesion was predominantly cystic and had a vivid peripherical post-contrastographic enhancement (**F**) with a solid component on the lateral side of the tumor; this region presented restricted diffusion on DWI confirmed by the ADC map (circle) (**G**,**H**), related to an increase in tumor cellularity. FLAIR = fluid-attenuated inversion recovery; DWI = diffusion-weighted imaging; ADC = apparent diffusion coefficient.

4. Lymphomas

One of the uses of DWI on CNS neoplasia imaging is the differential diagnosis between glioblastoma and primary CNS lymphoma (PCNSL), two entities that may appear similar on conventional imaging when considering a patient presenting with an enhancing brain mass but with a completely different pathogenesis, origin, and treatment [74,75]. PCNSLs are highly cellular tumors with relatively little extracellular space, which limits the diffusivity of free water. As a result, compared to HGGs and metastases, PCNSLs have been found to have much lower ADC values (Figure 3A–H). Similar to ADC, PCNSLs have been found to have lower FA values than high-grade gliomas [4,76–85].
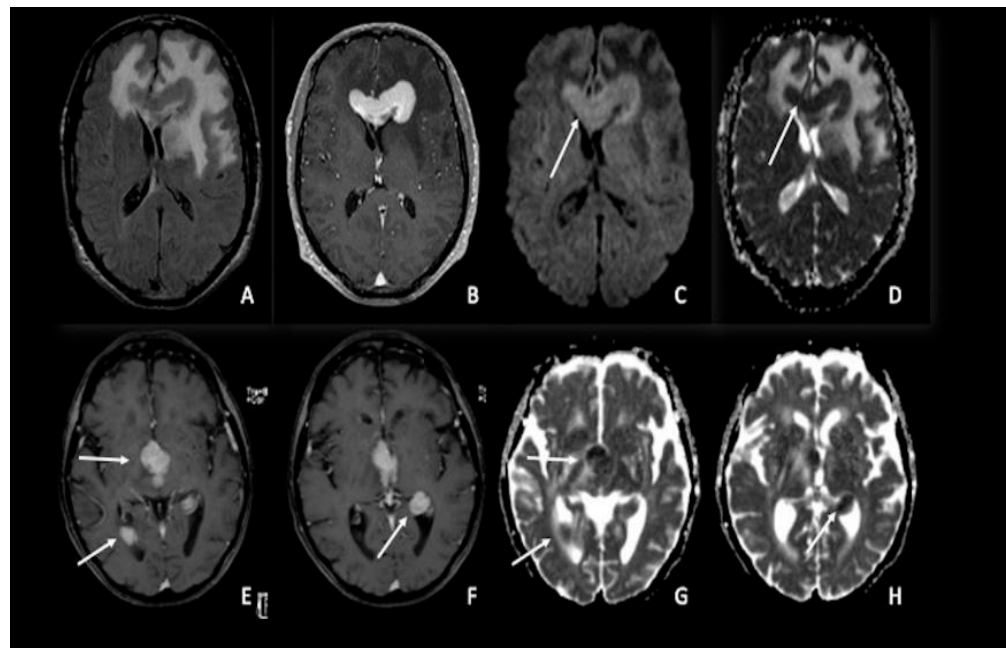
Figure 3. Two different cases of primitive cerebral lymphoma: the upper row showed a lymphoma in the pericallosal region (**A–D**) with a marked uniform enhancement on post-contrastographic T1 weighted image (**B**) and significant edema in the adjacent brain (**A**). The lower row showed a periventricular multicentric lymphoma (**E–H**) with multiple nodules of marked enhancement on post-contrast T1 weighted images (arrows) (**E**,**F**). Both cases presented restricted water diffusion with hyperintensity on DWI (arrow in **C**) and hypointense areas on ADC (arrows respectively in (**D**,**G**,**H**)), related to increasing tumor cellularity, as occurs typically in lymphomas. DWI = diffusion-weighted imaging; ADC = apparent diffusion coefficient.

5. Medulloblastomas

Medulloblastomas are highly cellular tumors; consequently, they present a substantial reduction in water molecule movement, resulting in a high diffusivity restriction on DWI and ADC images [86–103]. This finding helps in the differential diagnosis of other tumors typically located in the posterior fossa, such as ependymomas and pilocytic astrocytomas. Indeed, even if there is still overlap between these tumors [94,96,97,103–106], a high diffusion restriction is more suggestive of medulloblastomas than ependymomas or pilocytic astrocytomas [86,103,107] (Figure 4A–C). An ADC cut-off between 700 and 900 mm^2/s has been proposed by the literature to distinguish medulloblastomas from pilocytic astrocytomas [106,108,109], whereas using a minimum ADC cut-off value of 660 mm^2/s seems to allow for a good distinction with ependymomas [110]. Moreover, according to the literature, the ratio of ADC within the tumor compared to the grey matter ranges between 0.70 and 0.88 for the solid component [97,108,111] and 0.97 and 1.28 for the entire tumor [108,112–114]. Medulloblastomas, ependymomas, and pilocytic astrocytomas share the same fractional anisotropy [115–117]. As measured by lower ADC values, medulloblastomas frequently have lower rates of microscopic water diffusion than other common posterior fossa tumors in children [96]. This trait is most likely brought on by the frequent presence of cells with a high nuclear-to-cytoplasmic ratio and a high degree of cellularity in medulloblastomas, which results in additional membrane barriers impeding microscopic water diffusion [118]. Another much rarer tumor of the posterior fossa, typically affecting children, is the atypical teratoid/rhabdoid tumor (ATRT), which histologically resembles medulloblastoma [119] and exhibits similar DWI characteristics to medulloblastoma [86,111]. Finally, the distinction between medulloblastomas and glioblastomas cannot be made with DWI [86].
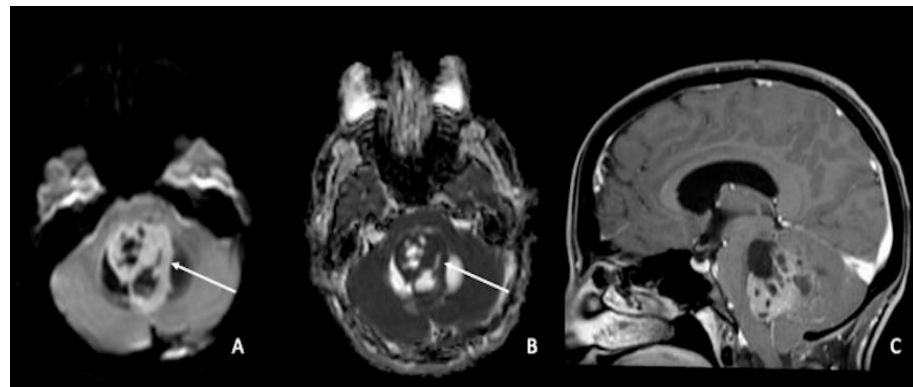
Figure 4. Medulloblastoma in a 30-year-old: (**A**,**C**) lesion of the posterior fossa with growth in the median line, close to the IV ventricle, characterized by inhomogeneous enhancement (arrow in (**A**)), mass effect, and (**B**) low ADC values (arrow). Using ADC values and a specific cut-off, it could be possible to distinguish medulloblastoma from ependymoma or pilocytic glioma. ADC = apparent diffusion coefficient.

According to Ahmed et al.'s study, the ADC ratio (ADC of the tumor divided by the ADC of the corresponding contralateral normal white matter) was unable to distinguish between medulloblastoma and ATRT. This could be explained by the fact that medulloblastoma and ATRT both have high grades in accordance with the WHO grading system, which indicates high tumoral cellularity and leads to a low ADC ratio [120].

6. Meningiomas and Vestibular Schwannomas

More than 30% of all brain tumors are meningiomas, which are the most frequent benign intracranial tumors [1]. Meningiomas are classified with three malignancy grades (WHO grades 1–3) in the 2016 World Health Organization (WHO) classification of central nervous system tumors [2] and are considered a single tumor type with 15 subtypes in the 2021 WHO classification. The more aggressive meningiomas are clinically characterized by more morbidity and mortality and have a higher chance of recurrence [3,4]. Tumor grading has a significant role in meningioma therapy planning. Adjuvant radiation is advised for high-grade meningiomas, while surgical excision is seen to be appropriate for low-grade meningiomas [5,6]. Therefore, accurate preoperative tumor grade prediction for meningiomas is essential in clinical practice.

Numerous studies have described the correlation between ADC values and the grading of meningiomas, with debated results. The ability of DWI to classify cellular malignancies has allowed it to characterize various meningioma subtypes. Except for heavily calcified or psammomatous meningiomas, atypical or malignant meningiomas have lower ADC and higher FA values than normal brain parenchyma [121–123] (Figure 5A,B). According to the WHO 2016 classification, meningiomas are graded based on the mitotic number and the invasive characteristics. The Ki-67 index is a crucial indicator of cellular proliferation, and research has shown a relationship between the Ki-67 index and the grading of meningiomas [124]. In addition, meningiomas with a higher Ki-67 index have a worse prognosis and a higher probability of tumor recurrence [125]. Numerous cancers' microstructural cellularity was demonstrated to be reflected by ADC values [126]. In fact, some authors claimed that ADC values could distinguish between low-grade and high-grade meningiomas by correlating inversely with the Ki-67 proliferation index [127]. This paper showed that mean ADC levels in high-grade meningiomas are substantially lower than in low-grade meningiomas. As a result, ADC may be a practical and non-invasive method for identifying low-grade and high-grade aggressive meningioma as well as for planning meningioma treatments, such as the degree of tumor resection, the application of adjuvant radiation, and the intervals for MRI follow-up [127]. The validation of an ADC threshold, however, was not observed in an older meta-analysis of 17 trials that were conducted to

differentiate between benign and high-grade meningiomas [128]. Diffusion MRI was also used to predict meningioma consistency, with debated results. Although Hoover et al. and Watanabe et al. did not find any association with tumor consistency [129,130], Yogi et al. discovered that hard meningiomas had considerably lower minimum ADC values than soft tumors [131]. Although they lacked histological confirmation, the authors concluded that tougher lesions are characterized by significant cellularity and fibrous material. Regarding the use of DTI, Kashimura et al. demonstrated that the FA values for hard meningiomas were significantly higher than those for soft meningiomas [132,133].
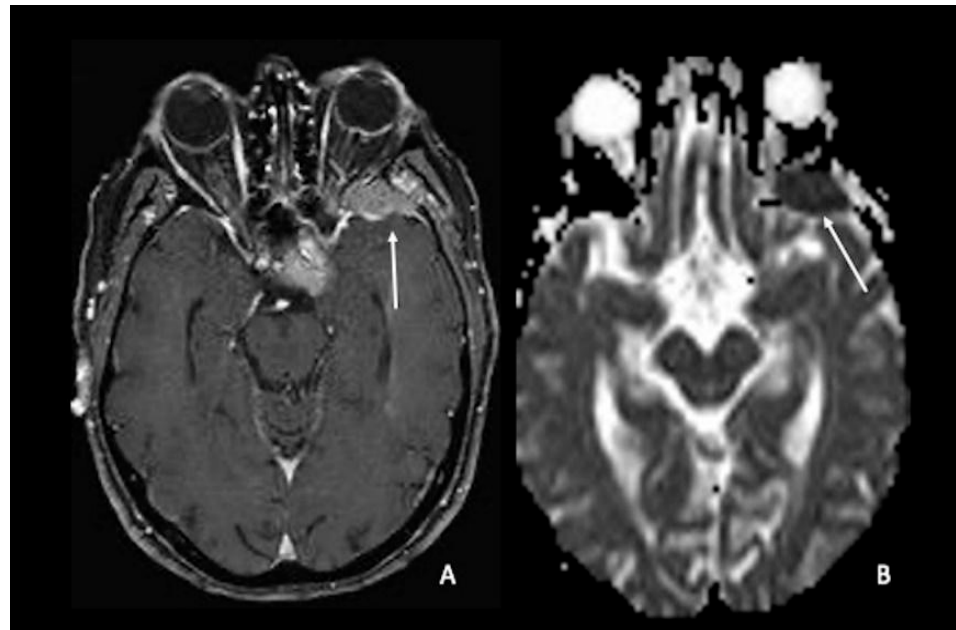

Figure 5. Aggressive meningioma: (**A**) atypical or malignant meningiomas (arrow) could have (**B**) lower ADC values than normal brain parenchyma (arrow). ADC = apparent diffusion coefficient.

Vestibular schwannomas (VSs) are the most common tumors in the cerebellopontine angle [134]. The therapeutic options for VSs include observation, surgery, and radiation therapy [135], depending on different variables such as the size at initial diagnosis, the tumor growth rate on serial imaging, and patient symptoms. Radiation therapy is usually the better choice for small to medium-sized VSs, with a lower rate of facial nerve palsy and hearing loss in comparison with surgery [136].

Another important clinical-radiological issue is the early assessment of tumor response to therapy. Morphologic and volumetric changes represent useful information in response to treatment. Anyway, it seems that in the acute phase after radiotherapy (from week 2 to week 8), there is an acute response characterized by cell swelling and disruption of the cytoarchitecture due to radiation that leads to an increase in terms of tumor volume, making the volumetric measures useless in the early post-radiotherapy assessment [137]. On the other hand, it seems that DWI and DTI could provide functional information about the response after radiotherapy in VSs, making them useful tools [137].

Indeed, a cut-off of 800×10^{-6} mm^2/s for minimum ADC values in VSs has been proposed to predict tumor response to radiotherapy with 90% accuracy, 77.8% sensitivity, and 100% specificity. All VSs from non-responders had ADC values greater than 800×10^{-6} mm^2/s. No statistically significant correlation with tumor response is evident when comparing ADC values before and after radiotherapy, perhaps due to tissue damage and vasogenic edema development [138]. Other authors reported that DTI could detect functional changes in response to stereotactic radiosurgery that preceded morphological modifications. Starting from week 12 after treatment, significant changes in VSs were

evident; a FA reduction and an ADC increase correspond, respectively, to disruption of the cytoarchitecture and necrosis [137].

7. Metastasis

Brain metastases are the most frequent central nervous system malignancies, often related to lung or breast cancer and less frequently related to cutaneous or intestinal tumors. Hematogenous spread is the most frequent way for cancer cells to move to the central nervous system. The spread of metastatic disease within the CNS follows different steps: first of all, there is the detachment of neoplastic cells from the primary tumor mass, then these cells enter the bloodstream with hematogenous disease dissemination to the metastatic site, and finally, there is the extravasation through the vascular wall and perivascular or brain parenchymal proliferation [139,140]. The ADC features of metastatic brain lesions and the distinction from primary tumors have only been the subject of a small number of studies, which may aid in distinguishing the origin of different brain metastases [141]. Restricted diffusion on DWI can be frequently found in intracerebral metastases, especially when the tumor is lung or breast cancer. The restriction of diffusion within a single brain metastasis may have been caused by an increase in the protein concentration in the form of highly viscous mucin [142] (Figure 6A,B). The pathology of metastases can be predicted by DWI signal intensity. On DWI sequences, adenocarcinomas (from the lung, ovary, and uterus) tend to be hypointense. Instead, hyperintense signals were seen in small- and large-cell neuroendocrine carcinomas [143]. Restricted diffusion was also observed in metastatic lesions of breast, colon, lung, and testis carcinomas, according to Duygulu et al. [142]. Studies have shown that small cell carcinomas (SCLC) tend to have low ADC values when compared to other tumors [144,145]. Other authors confirmed these results. Meyer et al. looked at 948 lesions from 159 patients, with malignant melanomas and lung and breast carcinomas being the most common types; due to lower values, ADC assessment allowed the differentiation of SCLC metastases from other tumors [146]. In another study, Zakaria et al. reported a negative correlation between cellularity and ADC values, with melanoma and SCLC having lower ADC values than metastases from other carcinomas (breast, ovarian, and colorectal malignancies) [147]. The genetic assessment of metastatic lesions may have an impact on the signal strength of lung cancer brain metastasis on DWI. Indeed, some authors find a significant correlation between ADC min and ADC ratio values and the presence or absence of EGFR mutations and their locations. In particular, low ADC values for lung adenocarcinoma-derived brain metastasis are linked to a high likelihood of an EGFR mutation, notably in exons 19 and 21 [148]. Multifocal, Dural-based enhancing lesions are the most frequent sign of metastatic disease to the dura.

Pachymeningeal carcinomatosis in tumors outside the CNS is uncommon; however, it most frequently manifests as hematogenous dissemination [149]. Pachymeningeal carcinomatosis is frequently caused by secondary leukemia, lymphoma, and metastatic breast, lung, and prostate cancers and shows restricted diffusion [139]. (Figure 7A–D).
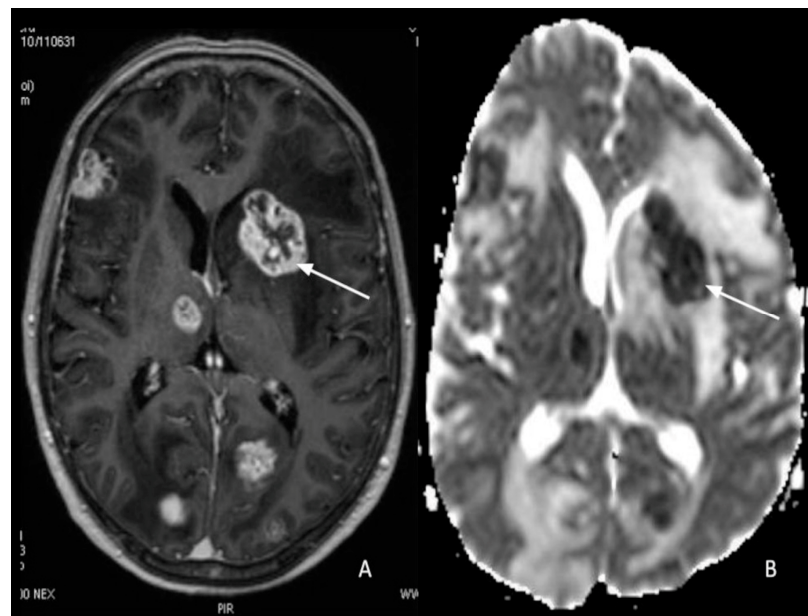
Figure 6. (**A**) Multiple enhancing metastatic lesions in a patient with lung cancer; (**B**) the reduced diffusion effect (arrow) is related to the high content of mucinous components.
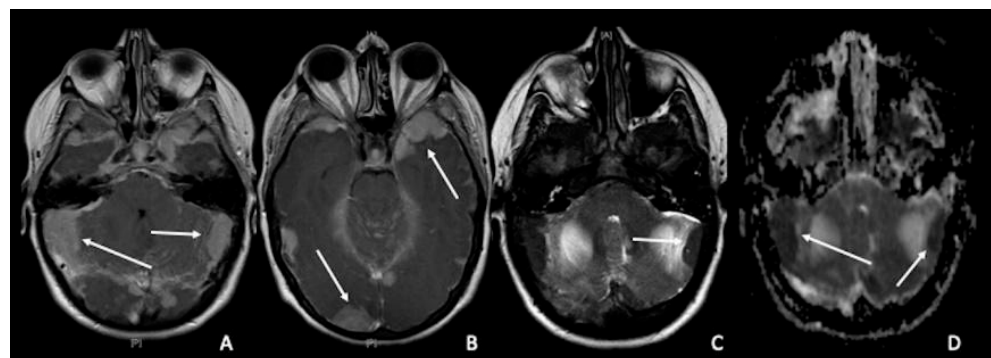

Figure 7. Multiple Chloromas (both supratentorial and infratentorial) in a patient with leukemia: (**A**,**B**) Pathologic extra-axial tissue enhancement after gadolinium (arrows) showed (**C**,**D**) restricted diffusion (arrows).

8. Gliomas vs. Metastasis

Diffusion imaging has also been used to discriminate glioblastoma from solitary brain metastases. Unfortunately, whereas tumoral ADC aids in tumor-type differentiation in some cases, it does not seem to be able to distinguish glioblastomas from metastases [13,150–152]. DWI can also be used to assess the ability of water molecules to move freely within non-enhancing peritumoral signal abnormalities (NEPSA) of CNS lesions. Neoplastic cells intermingled with areas of vasogenic edema within infiltrative NEPSA will create biological barriers that prevent the free passage of water molecules, resulting in lower ADC values than pure vasogenic edema [17]. Supporting this hypothesis, peritumoral ADC is lower in anaplastic astrocytoma and glioblastoma compared to metastases [151–154]. The non-infiltrative NEPSA vasogenic edema exhibits greater ADC values than the infiltrating NEPSA because there are no neoplastic cells to restrict the water molecules' movement [17]. Beyond the region of T2 signal abnormalities, analysis of ADC in the normal-appearing white matter has also been conducted. Patients with glioblastoma and metastases had distinct minimum ADC levels in their normal-appearing white matter; however, this method, in clinical use, was constrained by its underwhelming sensitivity and specificity (both around 70%) [151,155]. In the post-surgical setting, restricted diffusion aids in the detection

of cytotoxic edema [6]. Low ADC levels, which are also indicative of hypoxia (as observed in ischemic stroke or after surgery), suggest that variations in tumor hypoxia may affect tumor ADC values [156]. In the subacute setting, the associated parenchyma may enhance and be mistaken for tumor growth. Considering this, a baseline MRI is advised within 48 h of surgery [157]. Given the weaker ADC signal of the tumor, DWI can also be helpful for assessing treatment efficacy and distinguishing chemo-radiation-induced alterations from tumoral cells [6,158]. However, it is unknown what effect scarring and gliosis from chemotherapy or radiation have on ADC [129,156].

9. Post-Treatment Evaluation

Diffusion restriction inside a treated astrocytoma is likely associated with the recurrence and progression of the disease. Similarly, decreasing tumor burden correlates with increased diffusion during serial follow-up. ADC levels can also distinguish between post-radiation alterations (1.29–2.06, mean 1.570.35) and tumor growth (0.75–1.30, mean 1.140.18) [9,159]. A recent meta-analysis showed that DWI combined with MRI spectroscopy has very high sensitivity and specificity in differentiating recurrent glioma from radiation injury [160]. The current standard of care for patients with glioblastomas includes radiation (RT) and concurrent and adjuvant temozolomide (TMZ). The methylation state of the O-6-methylguanine-DNA methyltransferase (MGMT) gene promoter is a highly accurate predictor of the effectiveness of alchilant chemotherapy. As a molecular marker, MGMT is primarily used to assess how chemotherapy affects malignant gliomas and to identify new potential targets for tumor therapy [14,18,150,161]. Patients who showed methylation of the MGMT promoter had greater ADCmin values than those who did not, according to some authors, who also observed that the ADC ratio was much higher in the methylated group [15]. These authors assert that methylated MGMT tumors differ from unmethylated tumors in that they may be more varied or less cellular, less aggressive, and more amenable to therapy [15]. In previous research, DWI-ADC histogram values have been correlated with progression-free survival in glioblastoma patients. Specifically, broad and large histogram values predicted poor progression-free survival after surgery and radiochemotherapy [162]. MRI hyperintensity on T2 and fluid-attenuated inversion recovery (FLAIR) surrounding the enhancing portion of the tumor are common findings in higher-grade gliomas, which contain a combination of vasogenic edema and tumoral cells and are usually referred to as "non-contrast enhancing tumors" (NET) [163,164]. The analysis of this portion is essential in the evaluation of brain tumors as it may give valuable information on prognosis and tumor recurrence. Rathore et al. observed that on preoperative MRI, areas with increased rCBV and reduced ADC values were predictive of glioblastoma recurrence [165]. Moreover, a recent study found that ADC radiomic features on NET correlated with survival after >80% surgery and chemo/radiotherapy in younger patients (younger than 65 years old) [166].

10. Pituitary Adenoma

A pituitary adenoma is a common intracranial tumor that is preferably removed through transsphenoidal nasal surgery [167]. However, some characteristics hinder the possibility of this approach. Fibrous tumors, for instance, are difficult to remove by curettage and suction via this approach, usually requiring a second transcranial surgery [168]. Hence, assessing tumor consistency in the preoperative stage could be very important. Several studies investigated the correlation between DWI values and tumor consistency, with conflicting results [169–171]. Recent research evaluated macroadenomas' collagen content (which is high in a harder tumor), finding that lower ADC values were associated with higher collagen content [172,173]. Another study successfully differentiated between functional and non-functional macroadenomas by analyzing ADC histogram features [174]. In addition, ADC histogram values (skewness and kurtosis) have been proven useful in predicting macroadenoma proliferative potential and recurrence after surgery [175].

11. Skull Lesions

Skull lesions are often incidental findings and are associated with nonspecific symptoms [176]. If CT is a helpful tool for detecting bony lysis, sclerosis, and calcification within the lesion or its margins, MRI is superior to CT in the demonstration of soft tissue components and extraosseous involvement [177].

CT and MRI studies for the morphological evaluation of lesions do not always offer adequate answers to allow a correct diagnostic-therapeutic procedure to identify which lesions need treatment and which need follow-up [178]. Undefined margins, sclerotic margins, or cortical flaws may not always be able to discriminate between benign and cancerous tissue that involves the skull [177].

Among MR techniques, diffusion plays an important role in defining cellularity and allows us to distinguish tissues that are much more aggressive compared to benign ones. ADC values have been found to be much greater in benign skull tumors than in malignant lesions, suggesting that this parameter may help to focus the differential diagnosis for ambiguous diseases involving the skull [177].

Some authors reported that a threshold ADC value of 0.966×10^{-3} mm^2/s is useful to differentiate benign lesions from malignant lesions of the skull, with a good diagnostic value (AUC of 0.76) [179]. Nevertheless, some benign lesions with low ADC resulted in false positives, such as eosinophilic granulomas, epidermoid cysts, and the sclerotic variant of fibrous dysplasia. Other authors observed that the combination of conventional CT and MRI images with DWI could be applied to discriminate the skull base lesions where biopsies could be hazardous. The combination of CT, MRI, and DWI provided the best sensitivity for identifying benign from malignant skull lesions, whereas DWI alone provided the best specificity [177].

12. Conclusions

In conclusion, diffusion techniques, both conventional and advanced, have been proven useful in different applications in neuro-oncology imaging, ranging from differential diagnosis, histopathological composition, molecular profiling, prognosis, post-treatment response, and tumor recurrence. Being very common and easy to use in clinical practice, this sequence may be further implemented to help clinicians find new aspects of brain tumors and new therapeutic options.

References

1. Martín-Noguerol, T.; Mohan, S.; Santos-Armentia, E.; Cabrera-Zubizarreta, A.; Luna, A. Advanced MRI assessment of non-enhancing peritumoral signal abnormality in brain lesions. *Eur. J. Radiol.* **2021**, *143*, 109900. [CrossRef] [PubMed]
2. Martín Noguerol, T.; Martínez Barbero, J.P. Advanced diffusion MRI and biomarkers in the central nervous system: A new approach. *Radiologia* **2017**, *59*, 273–285. [CrossRef] [PubMed]
3. Huisman, T.A. Diffusion-weighted imaging: Basic concepts and application in cerebral stroke and head trauma. *Eur. Radiol.* **2003**, *13*, 2283–2297. [CrossRef] [PubMed]
4. Svolos, P.; Kousi, E.; Kapsalaki, E.; Theodorou, K.; Fezoulidis, I.; Kappas, C.; Tsougos, I. The role of diffusion and perfusion weighted imaging in the differential diagnosis of cerebral tumors: A review and future perspectives. *Cancer Imaging* **2014**, *14*, 20. [CrossRef] [PubMed]
5. Romano, A.; Bozzao, A.; Bonamini, M.; Fasoli, F.; Ferrante, M.; Floris, R.; Colonnese, C.; Fantozzi, L.M. Diffusion-weighted MR Imaging: Clinical applications in neuroradiology. *Radiol. Med.* **2003**, *106*, 521–548.

6.　Overcast, W.B.; Davis, K.M.; Ho, C.Y.; Hutchins, G.D.; Green, M.A.; Graner, B.D.; Veronesi, M.C. Advanced imaging techniques for neuro-oncologic tumor diagnosis, with an emphasis on PET-MRI imaging of malignant brain tumors. *Curr. Oncol. Rep.* **2021**, *23*, 34. [CrossRef] [PubMed]

7.　Dhermain, F.G.; Hau, P.; Lanfermann, H.; Jacobs, A.H.; van den Bent, M.J. Advanced MRI and PET imaging for assessment of treatment response in patients with gliomas. *Lancet Neurol.* **2010**, *9*, 906–920. [CrossRef] [PubMed]

8.　Falini, A.; Romano, A.; Bozzao, A. Tumours. *Neurol. Sci.* **2008**, *29* (Suppl. S3), 327–332. [CrossRef] [PubMed]

9.　Gaddamanugu, S.; Shafaat, O.; Sotoudeh, H.; Sarrami, A.H.; Rezaei, A.; Saadatpour, Z.; Singhal, A. Clinical applications of diffusion-weighted sequence in brain imaging: Beyond stroke. *Neuroradiology* **2022**, *64*, 15–30. [CrossRef]

10.　Guo, A.C.; Cummings, T.J.; Dash, R.C.; Provenzale, J.M. Lymphomas and high-grade astrocytomas: Comparison of water diffusibility and histologic characteristics. *Radiology* **2002**, *224*, 177–183. [CrossRef]

11.　Higano, S.; Yun, X.; Kumabe, T.; Watanabe, M.; Mugikura, S.; Umetsu, A.; Sato, A.; Yamada, T.; Takahashi, S. Malignant astrocytic tumors: Clinical importance of apparent diffusion coefficient in prediction of grade and prognosis. *Radiology* **2006**, *241*, 839–846. [CrossRef] [PubMed]

12.　Moon, W.J.; Choi, J.W.; Roh, H.G.; Lim, S.D.; Koh, Y.C. Imaging parameters of high grade gliomas in relation to the MGMT promoter methylation status: The CT, diffusion tensor imaging, and perfusion MR imaging. *Neuroradiology* **2012**, *54*, 555–563. [CrossRef] [PubMed]

13.　Yamasaki, F.; Kurisu, K.; Satoh, K.; Arita, K.; Sugiyama, K.; Ohtaki, M.; Takaba, J.; Tominaga, A.; Hanaya, R.; Yoshioka, H.; et al. Apparent diffusion coefficient of human brain tumors at MR imaging. *Radiology* **2005**, *235*, 985–991. [CrossRef] [PubMed]

14.　Murakami, R.; Sugahara, T.; Nakamura, H.; Hirai, T.; Kitajima, M.; Hayashida, Y.; Baba, Y.; Oya, N.; Kuratsu, J.; Yamashita, Y. Malignant supratentorial astrocytoma treated with postoperative radiation therapy: Prognostic value of pretreatment quantitative diffusion-weighted MR imaging. *Radiology* **2007**, *243*, 493–499. [CrossRef] [PubMed]

15.　Romano, A.; Calabria, L.F.; Tavanti, F.; Minniti, G.; Rossi-Espagnet, M.C.; Coppola, V.; Pugliese, S.; Guida, D.; Francione, G.; Colonnese, C.; et al. Apparent diffusion coefficient obtained by magnetic resonance imaging as a prognostic marker in glioblastomas: Correlation with MGMT promoter methylation status. *Eur. Radiol.* **2013**, *23*, 513–520. [CrossRef] [PubMed]

16.　Silber, J.R.; Blank, A.; Bobola, M.S.; Ghatan, S.; Kolstoe, D.D.; Berger, M.S. O6-methylguanine-DNA methyltransferase-deficient phenotype in human gliomas: Frequency and time to tumor progression after alkylating agent-based chemotherapy. *Clin. Cancer Res.* **1999**, *5*, 807–814.

17.　Sugahara, T.; Korogi, Y.; Kochi, M.; Ikushima, I.; Shigematu, Y.; Hirai, T.; Okuda, T.; Liang, L.; Ge, Y.; Komohara, Y.; et al. Usefulness of diffusion-weighted MRI with echo-planar technique in the evaluation of cellularity in gliomas. *J. Magn. Reson. Imaging* **1999**, *9*, 53–60. [CrossRef]

18.　Gupta, R.K.; Cloughesy, T.F.; Sinha, U.; Garakian, J.; Lazareff, J.; Rubino, G.; Rubino, L.; Becker, D.P.; Vinters, H.V.; Alger, J.R. Relationships between choline magnetic resonance spectroscopy, apparent diffusion coefficient and quantitative histopathology in human glioma. *J. Neurooncol.* **2000**, *50*, 215–226. [CrossRef]

19.　Qin, J.B.; Zhang, H.; Wang, X.C.; Tan, Y.; Wu, X.F. Combination value of diffusion-weighted imaging and dynamic susceptibility contrast-enhanced MRI in astrocytoma grading and correlation with GFAP, Topoisomerase IIα and MGMT. *Oncol. Lett.* **2019**, *18*, 2763–2770. [CrossRef]

20.　Wang, Q.P.; Lei, D.Q.; Yuan, Y.; Xiong, N.X. Accuracy of ADC derived from DWI for differentiating high-grade from low-grade gliomas: Systematic review and meta-analysis. *Medicine* **2020**, *99*, e19254. [CrossRef]

21.　Van Cauter, S.; Veraart, J.; Sijbers, J.; Peeters, R.R.; Himmelreich, U.; De Keyzer, F.; Van Gool, S.W.; Van Calenbergh, F.; De Vleeschouwer, S.; Van Hecke, W.; et al. Gliomas: Diffusion kurtosis MR imaging in grading. *Radiology* **2012**, *263*, 492–501. [CrossRef] [PubMed]

22.　Alexander, A.L.; Lee, J.E.; Lazar, M.; Field, A.S. Diffusion tensor imaging of the brain. *Neurotherapeutics* **2007**, *4*, 316–329. [CrossRef] [PubMed]

23.　Jensen, J.H.; Helpern, J.A. MRI quantification of non-Gaussian water diffusion by kurtosis analysis. *NMR Biomed.* **2010**, *23*, 698–710. [CrossRef] [PubMed]

24.　Raab, P.; Hattingen, E.; Franz, K.; Zanella, F.E.; Lanfermann, H. Cerebral gliomas: Diffusional kurtosis imaging analysis of microstructural differences. *Radiology* **2010**, *254*, 876–881. [CrossRef] [PubMed]

25.　Abdalla, G.; Dixon, L.; Sanverdi, E.; Machado, P.M.; Kwong, J.S.W.; Panovska-Griffiths, J.; Rojas-Garcia, A.; Yoneoka, D.; Veraart, J.; Van Cauter, S.; et al. The diagnostic role of diffusional kurtosis imaging in glioma grading and differentiation of gliomas from other intra-axial brain tumours: A systematic review with critical appraisal and meta-analysis. *Neuroradiology* **2020**, *62*, 791–802. [CrossRef] [PubMed]

26.　Wen, Q.; Kelley, D.A.; Banerjee, S.; Lupo, J.M.; Chang, S.M.; Xu, D.; Hess, C.P.; Nelson, S.J. Clinically feasible NODDI characterization of glioma using multiband EPI at 7 T. *Neuroimage Clin.* **2015**, *9*, 291–299. [CrossRef] [PubMed]

27.　Louis, D.N.; Perry, A.; Reifenberger, G.; von Deimling, A.; Figarella-Branger, D.; Cavenee, W.K.; Ohgaki, H.; Wiestler, O.D.; Kleihues, P.; Ellison, D.W. The 2016 World Health Organization Classification of Tumors of the Central Nervous System: A summary. *Acta Neuropathol.* **2016**, *131*, 803–820. [CrossRef] [PubMed]

28.　Appin, C.L.; Brat, D.J. Molecular genetics of gliomas. *Cancer J.* **2014**, *20*, 66–72. [CrossRef]

29. Louis, D.N.; Perry, A.; Wesseling, P.; Brat, D.J.; Cree, I.A.; Figarella-Branger, D.; Hawkins, C.; Ng, H.K.; Pfister, S.M.; Reifenberger, G.; et al. The 2021 WHO Classification of Tumors of the Central Nervous System: A summary. *Neuro-Oncology* **2021**, *23*, 1231–1251. [CrossRef]

30. Kickingereder, P.; Sahm, F.; Radbruch, A.; Wick, W.; Heiland, S.; Deimling, A.V.; Bendszus, M.; Wiestler, B. IDH mutation status is associated with a distinct hypoxia/angiogenesis transcriptome signature which is non-invasively predictable with rCBV imaging in human glioma. *Sci. Rep.* **2015**, *5*, 16238. [CrossRef]

31. Brat, D.J.; Verhaak, R.G.; Aldape, K.D.; Yung, W.K.; Salama, S.R.; Cooper, L.A.; Rheinbay, E.; Miller, C.R.; Vitucci, M.; Morozova, O.; et al. Comprehensive, Integrative Genomic Analysis of Diffuse Lower-Grade Gliomas. *N. Engl. J. Med.* **2015**, *372*, 2481–2498. [CrossRef] [PubMed]

32. Miller, J.J.; Shih, H.A.; Andronesi, O.C.; Cahill, D.P. Isocitrate dehydrogenase-mutant glioma: Evolving clinical and therapeutic implications. *Cancer* **2017**, *123*, 4535–4546. [CrossRef] [PubMed]

33. Yu, J.; Shi, Z.; Lian, Y.; Li, Z.; Liu, T.; Gao, Y.; Wang, Y.; Chen, L.; Mao, Y. Noninvasive IDH1 mutation estimation based on a quantitative radiomics approach for grade II glioma. *Eur. Radiol.* **2017**, *27*, 3509–3522. [CrossRef] [PubMed]

34. Suh, C.H.; Kim, H.S.; Jung, S.C.; Choi, C.G.; Kim, S.J. Imaging prediction of isocitrate dehydrogenase (IDH) mutation in patients with glioma: A systemic review and meta-analysis. *Eur. Radiol.* **2019**, *29*, 745–758. [CrossRef] [PubMed]

35. van den Bent, M.J.; Brandes, A.A.; Taphoorn, M.J.; Kros, J.M.; Kouwenhoven, M.C.; Delattre, J.Y.; Bernsen, H.J.; Frenay, M.; Tijssen, C.C.; Grisold, W.; et al. Adjuvant procarbazine, lomustine, and vincristine chemotherapy in newly diagnosed anaplastic oligodendroglioma: Long-term follow-up of EORTC brain tumor group study 26951. *J. Clin. Oncol.* **2013**, *31*, 344–350. [CrossRef]

36. Chamberlain, M.C.; Born, D. Prognostic significance of relative 1p/19q codeletion in oligodendroglial tumors. *J. Neurooncol.* **2015**, *125*, 249–251. [CrossRef]

37. Wu, C.C.; Jain, R.; Radmanesh, A.; Poisson, L.M.; Guo, W.Y.; Zagzag, D.; Snuderl, M.; Placantonakis, D.G.; Golfinos, J.; Chi, A.S. Predicting Genotype and Survival in Glioma Using Standard Clinical MR Imaging Apparent Diffusion Coefficient Images: A Pilot Study from the Cancer Genome Atlas. *AJNR Am. J. Neuroradiol.* **2018**, *39*, 1814–1820. [CrossRef]

38. Dang, L.; Yen, K.; Attar, E.C. IDH mutations in cancer and progress toward development of targeted therapeutics. *Ann. Oncol.* **2016**, *27*, 599–608. [CrossRef]

39. Zhou, H.; Vallières, M.; Bai, H.X.; Su, C.; Tang, H.; Oldridge, D.; Zhang, Z.; Xiao, B.; Liao, W.; Tao, Y.; et al. MRI features predict survival and molecular markers in diffuse lower-grade gliomas. *Neuro-Oncology* **2017**, *19*, 862–870. [CrossRef]

40. Zhang, B.; Chang, K.; Ramkissoon, S.; Tanguturi, S.; Bi, W.L.; Reardon, D.A.; Ligon, K.L.; Alexander, B.M.; Wen, P.Y.; Huang, R.Y. Multimodal MRI features predict isocitrate dehydrogenase genotype in high-grade gliomas. *Neuro-Oncology* **2017**, *19*, 109–117. [CrossRef]

41. Xing, Z.; Yang, X.; She, D.; Lin, Y.; Zhang, Y.; Cao, D. Noninvasive Assessment of IDH Mutational Status in World Health Organization Grade II and III Astrocytomas Using DWI and DSC-PWI Combined with Conventional MR Imaging. *AJNR Am. J. Neuroradiol.* **2017**, *38*, 1138–1144. [CrossRef] [PubMed]

42. Tietze, A.; Choi, C.; Mickey, B.; Maher, E.A.; Parm Ulhøi, B.; Sangill, R.; Lassen-Ramshad, Y.; Lukacova, S.; Østergaard, L.; von Oettingen, G. Noninvasive assessment of isocitrate dehydrogenase mutation status in cerebral gliomas by magnetic resonance spectroscopy in a clinical setting. *J. Neurosurg.* **2018**, *128*, 391–398. [CrossRef] [PubMed]

43. Tan, W.; Xiong, J.; Huang, W.; Wu, J.; Zhan, S.; Geng, D. Noninvasively detecting Isocitrate dehydrogenase 1 gene status in astrocytoma by dynamic susceptibility contrast MRI. *J. Magn. Reson. Imaging* **2017**, *45*, 492–499. [CrossRef] [PubMed]

44. Stadlbauer, A.; Zimmermann, M.; Kitzwögerer, M.; Oberndorfer, S.; Rössler, K.; Dörfler, A.; Buchfelder, M.; Heinz, G. MR Imaging-derived Oxygen Metabolism and Neovascularization Characterization for Grading and IDH Gene Mutation Detection of Gliomas. *Radiology* **2017**, *283*, 799–809. [CrossRef] [PubMed]

45. Price, S.J.; Allinson, K.; Liu, H.; Boonzaier, N.R.; Yan, J.L.; Lupson, V.C.; Larkin, T.J. Less Invasive Phenotype Found in Isocitrate Dehydrogenase-mutated Glioblastomas than in Isocitrate Dehydrogenase Wild-Type Glioblastomas: A Diffusion-Tensor Imaging Study. *Radiology* **2017**, *283*, 215–221. [CrossRef]

46. Patel, S.H.; Poisson, L.M.; Brat, D.J.; Zhou, Y.; Cooper, L.; Snuderl, M.; Thomas, C.; Franceschi, A.M.; Griffith, B.; Flanders, A.E.; et al. T2-FLAIR Mismatch, an Imaging Biomarker for IDH and 1p/19q Status in Lower-grade Gliomas: A TCGA/TCIA Project. *Clin. Cancer Res.* **2017**, *23*, 6078–6085. [CrossRef]

47. Nakae, S.; Murayama, K.; Sasaki, H.; Kumon, M.; Nishiyama, Y.; Ohba, S.; Adachi, K.; Nagahisa, S.; Hayashi, T.; Inamasu, J.; et al. Prediction of genetic subgroups in adult supra tentorial gliomas by pre- and intraoperative parameters. *J. Neurooncol.* **2017**, *131*, 403–412. [CrossRef]

48. Leu, K.; Ott, G.A.; Lai, A.; Nghiemphu, P.L.; Pope, W.B.; Yong, W.H.; Liau, L.M.; Cloughesy, T.F.; Ellingson, B.M. Perfusion and diffusion MRI signatures in histologic and genetic subtypes of WHO grade II-III diffuse gliomas. *J. Neurooncol.* **2017**, *134*, 177–188. [CrossRef]

49. Lasocki, A.; Tsui, A.; Gaillard, F.; Tacey, M.; Drummond, K.; Stuckey, S. Reliability of noncontrast-enhancing tumor as a biomarker of IDH1 mutation status in glioblastoma. *J. Clin. Neurosci.* **2017**, *39*, 170–175. [CrossRef]

50. Jiang, S.; Zou, T.; Eberhart, C.G.; Villalobos, M.A.V.; Heo, H.Y.; Zhang, Y.; Wang, Y.; Wang, X.; Yu, H.; Du, Y.; et al. Predicting IDH mutation status in grade II gliomas using amide proton transfer-weighted (APTw) MRI. *Magn. Reson. Med.* **2017**, *78*, 1100–1109. [CrossRef]

51. Hsieh, K.L.; Chen, C.Y.; Lo, C.M. Radiomic model for predicting mutations in the isocitrate dehydrogenase gene in glioblastomas. *Oncotarget* **2017**, *8*, 45888–45897. [CrossRef] [PubMed]

52. Hempel, J.M.; Schittenhelm, J.; Brendle, C.; Bender, B.; Bier, G.; Skardelly, M.; Tabatabai, G.; Castaneda Vega, S.; Ernemann, U.; Klose, U. Histogram analysis of diffusion kurtosis imaging estimates for in vivo assessment of 2016 WHO glioma grades: A cross-sectional observational study. *Eur. J. Radiol.* **2017**, *95*, 202–211. [CrossRef] [PubMed]

53. Grabner, G.; Kiesel, B.; Wöhrer, A.; Millesi, M.; Wurzer, A.; Göd, S.; Mallouhi, A.; Knosp, E.; Marosi, C.; Trattnig, S.; et al. Local image variance of 7 Tesla SWI is a new technique for preoperative characterization of diffusely infiltrating gliomas: Correlation with tumour grade and IDH1 mutational status. *Eur. Radiol.* **2017**, *27*, 1556–1567. [CrossRef] [PubMed]

54. Delfanti, R.L.; Piccioni, D.E.; Handwerker, J.; Bahrami, N.; Krishnan, A.; Karunamuni, R.; Hattangadi-Gluth, J.A.; Seibert, T.M.; Srikant, A.; Jones, K.A.; et al. Imaging correlates for the 2016 update on WHO classification of grade II/III gliomas: Implications for IDH, 1p/19q and ATRX status. *J. Neurooncol.* **2017**, *135*, 601–609. [CrossRef]

55. Yamashita, K.; Hiwatashi, A.; Togao, O.; Kikuchi, K.; Hatae, R.; Yoshimoto, K.; Mizoguchi, M.; Suzuki, S.O.; Yoshiura, T.; Honda, H. MR Imaging-Based Analysis of Glioblastoma Multiforme: Estimation of IDH1 Mutation Status. *AJNR Am. J. Neuroradiol.* **2016**, *37*, 58–65. [CrossRef]

56. Xiong, J.; Tan, W.; Wen, J.; Pan, J.; Wang, Y.; Zhang, J.; Geng, D. Combination of diffusion tensor imaging and conventional MRI correlates with isocitrate dehydrogenase 1/2 mutations but not 1p/19q genotyping in oligodendroglial tumours. *Eur. Radiol.* **2016**, *26*, 1705–1715. [CrossRef]

57. Wang, K.; Wang, Y.; Fan, X.; Wang, J.; Li, G.; Ma, J.; Ma, J.; Jiang, T.; Dai, J. Radiological features combined with IDH1 status for predicting the survival outcome of glioblastoma patients. *Neuro-Oncology* **2016**, *18*, 589–597. [CrossRef]

58. Choi, C.; Raisanen, J.M.; Ganji, S.K.; Zhang, S.; McNeil, S.S.; An, Z.; Madan, A.; Hatanpaa, K.J.; Vemireddy, V.; Sheppard, C.A.; et al. Prospective Longitudinal Analysis of 2-Hydroxyglutarate Magnetic Resonance Spectroscopy Identifies Broad Clinical Utility for the Management of Patients with IDH-Mutant Glioma. *J. Clin. Oncol.* **2016**, *34*, 4030–4039. [CrossRef]

59. Biller, A.; Badde, S.; Nagel, A.; Neumann, J.O.; Wick, W.; Hertenstein, A.; Bendszus, M.; Sahm, F.; Benkhedah, N.; Kleesiek, J. Improved Brain Tumor Classification by Sodium MR Imaging: Prediction of IDH Mutation Status and Tumor Progression. *AJNR Am. J. Neuroradiol.* **2016**, *37*, 66–73. [CrossRef]

60. Wasserman, J.K.; Nicholas, G.; Yaworski, R.; Wasserman, A.M.; Woulfe, J.M.; Jansen, G.H.; Chakraborty, S.; Nguyen, T.B. Radiological and pathological features associated with IDH1-R132H mutation status and early mortality in newly diagnosed anaplastic astrocytic tumours. *PLoS ONE* **2015**, *10*, e0123890. [CrossRef]

61. Sonoda, Y.; Shibahara, I.; Kawaguchi, T.; Saito, R.; Kanamori, M.; Watanabe, M.; Suzuki, H.; Kumabe, T.; Tominaga, T. Association between molecular alterations and tumor location and MRI characteristics in anaplastic gliomas. *Brain Tumor Pathol.* **2015**, *32*, 99–104. [CrossRef] [PubMed]

62. Lee, S.; Choi, S.H.; Ryoo, I.; Yoon, T.J.; Kim, T.M.; Lee, S.H.; Park, C.K.; Kim, J.H.; Sohn, C.H.; Park, S.H.; et al. Evaluation of the microenvironmental heterogeneity in high-grade gliomas with IDH1/2 gene mutation using histogram analysis of diffusion-weighted imaging and dynamic-susceptibility contrast perfusion imaging. *J. Neurooncol.* **2015**, *121*, 141–150. [CrossRef] [PubMed]

63. Reyes-Botero, G.; Dehais, C.; Idbaih, A.; Martin-Duverneuil, N.; Lahutte, M.; Carpentier, C.; Letouzé, E.; Chinot, O.; Loiseau, H.; Honnorat, J.; et al. Contrast enhancement in 1p/19q-codeleted anaplastic oligodendrogliomas is associated with 9p loss, genomic instability, and angiogenic gene expression. *Neuro-Oncology* **2014**, *16*, 662–670. [CrossRef] [PubMed]

64. Qi, S.; Yu, L.; Li, H.; Ou, Y.; Qiu, X.; Ding, Y.; Han, H.; Zhang, X. Isocitrate dehydrogenase mutation is associated with tumor location and magnetic resonance imaging characteristics in astrocytic neoplasms. *Oncol Lett.* **2014**, *7*, 1895–1902. [CrossRef] [PubMed]

65. Carrillo, J.A.; Lai, A.; Nghiemphu, P.L.; Kim, H.J.; Phillips, H.S.; Kharbanda, S.; Moftakhar, P.; Lalaezari, S.; Yong, W.; Ellingson, B.M.; et al. Relationship between tumor enhancement, edema, IDH1 mutational status, MGMT promoter methylation, and survival in glioblastoma. *AJNR Am. J. Neuroradiol.* **2012**, *33*, 1349–1355. [CrossRef]

66. Lee, E.J.; Lee, S.K.; Agid, R.; Bae, J.M.; Keller, A.; Terbrugge, K. Preoperative grading of presumptive low-grade astrocytomas on MR imaging: Diagnostic value of minimum apparent diffusion coefficient. *AJNR Am. J. Neuroradiol.* **2008**, *29*, 1872–1877. [CrossRef]

67. Fellah, S.; Caudal, D.; De Paula, A.M.; Dory-Lautrec, P.; Figarella-Branger, D.; Chinot, O.; Metellus, P.; Cozzone, P.J.; Confort-Gouny, S.; Ghattas, B.; et al. Multimodal MR imaging (diffusion, perfusion, and spectroscopy): Is it possible to distinguish oligodendroglial tumor grade and 1p/19q codeletion in the pretherapeutic diagnosis? *AJNR Am. J. Neuroradiol.* **2013**, *34*, 1326–1333. [CrossRef]

68. Jenkinson, M.D.; Smith, T.S.; Brodbelt, A.R.; Joyce, K.A.; Warnke, P.C.; Walker, C. Apparent diffusion coefficients in oligodendroglial tumors characterized by genotype. *J. Magn. Reson. Imaging* **2007**, *26*, 1405–1412. [CrossRef]

69. Park, Y.W.; Han, K.; Ahn, S.S.; Bae, S.; Choi, Y.S.; Chang, J.H.; Kim, S.H.; Kang, S.G.; Lee, S.K. Prediction of IDH1-Mutation and 1p/19q-Codeletion Status Using Preoperative MR Imaging Phenotypes in Lower Grade Gliomas. *AJNR Am. J. Neuroradiol.* **2018**, *39*, 37–42. [CrossRef]

70. Eichinger, P.; Alberts, E.; Delbridge, C.; Trebeschi, S.; Valentinitsch, A.; Bette, S.; Huber, T.; Gempt, J.; Meyer, B.; Schlegel, J.; et al. Diffusion tensor image features predict IDH genotype in newly diagnosed WHO grade II/III gliomas. *Sci. Rep.* **2017**, *7*, 13396. [CrossRef]

71. Figini, M.; Riva, M.; Graham, M.; Castelli, G.M.; Fernandes, B.; Grimaldi, M.; Baselli, G.; Pessina, F.; Bello, L.; Zhang, H.; et al. Prediction of Isocitrate Dehydrogenase Genotype in Brain Gliomas with MRI: Single-Shell versus Multishell Diffusion Models. *Radiology* **2018**, *289*, 788–796. [CrossRef] [PubMed]

72. Gao, A.; Zhang, H.; Yan, X.; Wang, S.; Chen, Q.; Gao, E.; Qi, J.; Bai, J.; Zhang, Y.; Cheng, J. Whole-Tumor Histogram Analysis of Multiple Diffusion Metrics for Glioma Genotyping. *Radiology* **2022**, *302*, 652–661. [CrossRef] [PubMed]

73. Park, Y.W.; Ahn, S.S.; Park, C.J.; Han, K.; Kim, E.H.; Kang, S.G.; Chang, J.H.; Kim, S.H.; Lee, S.K. Diffusion and perfusion MRI may predict EGFR amplification and the TERT promoter mutation status of IDH-wildtype lower-grade gliomas. *Eur. Radiol.* **2020**, *30*, 6475–6484. [CrossRef] [PubMed]

74. Drake-Pérez, M.; Boto, J.; Fitsiori, A.; Lovblad, K.; Vargas, M.I. Clinical applications of diffusion weighted imaging in neuroradiology. *Insights Imaging* **2018**, *9*, 535–547. [CrossRef] [PubMed]

75. Lin, X.; Lee, M.; Buck, O.; Woo, K.M.; Zhang, Z.; Hatzoglou, V.; Omuro, A.; Arevalo-Perez, J.; Thomas, A.A.; Huse, J.; et al. Diagnostic Accuracy of T1-Weighted Dynamic Contrast-Enhanced-MRI and DWI-ADC for Differentiation of Glioblastoma and Primary CNS Lymphoma. *AJNR Am. J. Neuroradiol.* **2017**, *38*, 485–491. [CrossRef] [PubMed]

76. Wang, S.; Kim, S.; Chawla, S.; Wolf, R.L.; Knipp, D.E.; Vossough, A.; O'Rourke, D.M.; Judy, K.D.; Poptani, H.; Melhem, E.R. Differentiation between glioblastomas, solitary brain metastases, and primary cerebral lymphomas using diffusion tensor and dynamic susceptibility contrast-enhanced MR imaging. *AJNR Am. J. Neuroradiol.* **2011**, *32*, 507–514. [CrossRef] [PubMed]

77. Toh, C.H.; Castillo, M.; Wong, A.M.; Wei, K.C.; Wong, H.F.; Ng, S.H.; Wan, Y.L. Primary cerebral lymphoma and glioblastoma multiforme: Differences in diffusion characteristics evaluated with diffusion tensor imaging. *AJNR Am. J. Neuroradiol.* **2008**, *29*, 471–475. [CrossRef]

78. Lu, X.; Xu, W.; Wei, Y.; Li, T.; Gao, L.; Fu, X.; Yao, Y.; Wang, L. Diagnostic performance of DWI for differentiating primary central nervous system lymphoma from glioblastoma: A systematic review and meta-analysis. *Neurol. Sci.* **2019**, *40*, 947–956. [CrossRef]

79. Ahn, S.J.; Shin, H.J.; Chang, J.H.; Lee, S.K. Differentiation between primary cerebral lymphoma and glioblastoma using the apparent diffusion coefficient: Comparison of three different ROI methods. *PLoS ONE* **2014**, *9*, e112948. [CrossRef]

80. Horger, M.; Fenchel, M.; Nägele, T.; Moehle, R.; Claussen, C.D.; Beschorner, R.; Ernemann, U. Water diffusivity: Comparison of primary CNS lymphoma and astrocytic tumor infiltrating the corpus callosum. *AJR Am. J. Roentgenol.* **2009**, *193*, 1384–1387. [CrossRef]

81. Calli, C.; Kitis, O.; Yunten, N.; Yurtseven, T.; Islekel, S.; Akalin, T. Perfusion and diffusion MR imaging in enhancing malignant cerebral tumors. *Eur. J. Radiol.* **2006**, *58*, 394–403. [CrossRef] [PubMed]

82. Server, A.; Kulle, B.; Maehlen, J.; Josefsen, R.; Schellhorn, T.; Kumar, T.; Langberg, C.W.; Nakstad, P.H. Quantitative apparent diffusion coefficients in the characterization of brain tumors and associated peritumoral edema. *Acta Radiol.* **2009**, *50*, 682–689. [CrossRef] [PubMed]

83. Rizzo, L.; Crasto, S.G.; Moruno, P.G.; Cassoni, P.; Rudà, R.; Boccaletti, R.; Brosio, M.; De Lucchi, R.; Fava, C. Role of diffusion- and perfusion-weighted MR imaging for brain tumour characterisation. *Radiol. Med.* **2009**, *114*, 645–659. [CrossRef] [PubMed]

84. Kinoshita, M.; Hashimoto, N.; Goto, T.; Kagawa, N.; Kishima, H.; Izumoto, S.; Tanaka, H.; Fujita, N.; Yoshimine, T. Fractional anisotropy and tumor cell density of the tumor core show positive correlation in diffusion tensor magnetic resonance imaging of malignant brain tumors. *Neuroimage* **2008**, *43*, 29–35. [CrossRef] [PubMed]

85. Rollin, N.; Guyotat, J.; Streichenberger, N.; Honnorat, J.; Tran Minh, V.A.; Cotton, F. Clinical relevance of diffusion and perfusion magnetic resonance imaging in assessing intra-axial brain tumors. *Neuroradiology* **2006**, *48*, 150–159. [CrossRef]

86. Yamashita, Y.; Kumabe, T.; Higano, S.; Watanabe, M.; Tominaga, T. Minimum apparent diffusion coefficient is significantly correlated with cellularity in medulloblastomas. *Neurol. Res.* **2009**, *31*, 940–946. [CrossRef]

87. Poussaint, T.Y.; Panigrahy, A.; Huisman, T.A. Pediatric brain tumors. *Pediatr. Radiol.* **2015**, *45* (Suppl. S3), S443–S453. [CrossRef]

88. Rasalkar, D.D.; Chu, W.C.; Paunipagar, B.K.; Cheng, F.W.; Li, C.K. Paediatric intra-axial posterior fossa tumours: Pictorial review. *Postgrad. Med. J.* **2013**, *89*, 39–46. [CrossRef]

89. Fruehwald-Pallamar, J.; Puchner, S.B.; Rossi, A.; Garre, M.L.; Cama, A.; Koelblinger, C.; Osborn, A.G.; Thurnher, M.M. Magnetic resonance imaging spectrum of medulloblastoma. *Neuroradiology* **2011**, *53*, 387–396. [CrossRef]

90. Plaza, M.J.; Borja, M.J.; Altman, N.; Saigal, G. Conventional and advanced MRI features of pediatric intracranial tumors: Posterior fossa and suprasellar tumors. *AJR Am. J. Roentgenol.* **2013**, *200*, 1115–1124. [CrossRef]

91. Eran, A.; Ozturk, A.; Aygun, N.; Izbudak, I. Medulloblastoma: Atypical CT and MRI findings in children. *Pediatr. Radiol.* **2010**, *40*, 1254–1262. [CrossRef] [PubMed]

92. Sarrazin, J.L. Tumeurs de la fosse postérieure [Infra tentorial tumors]. *J. Radiol.* **2006**, *87 Pt 2*, 748–763. [CrossRef] [PubMed]

93. Chawla, A.; Emmanuel, J.V.; Seow, W.T.; Lou, J.; Teo, H.E.; Lim, C.C. Paediatric PNET: Pre-surgical MRI features. *Clin. Radiol.* **2007**, *62*, 43–52. [CrossRef] [PubMed]

94. Schneider, J.F.; Confort-Gouny, S.; Viola, A.; Le Fur, Y.; Viout, P.; Bennathan, M.; Chapon, F.; Figarella-Branger, D.; Cozzone, P.; Girard, N. Multiparametric differentiation of posterior fossa tumors in children using diffusion-weighted imaging and short echo-time 1H-MR spectroscopy. *J. Magn. Reson. Imaging* **2007**, *26*, 1390–1398. [CrossRef] [PubMed]

95. Wu, G.; Pang, H.; Ghimire, P.; Liu, G. (1)H magnetic resonance spectroscopy and diffusion weighted imaging findings of medulloblastoma in 3.0T MRI: A retrospective analysis of 17 cases. *Neural. Regen. Res.* **2012**, *7*, 2554–2559. [CrossRef]

96. Bull, J.G.; Saunders, D.E.; Clark, C.A. Discrimination of paediatric brain tumours using apparent diffusion coefficient histograms. *Eur. Radiol.* **2012**, *22*, 447–457. [CrossRef]

97. Gimi, B.; Cederberg, K.; Derinkuyu, B.; Gargan, L.; Koral, K.M.; Bowers, D.C.; Koral, K. Utility of apparent diffusion coefficient ratios in distinguishing common pediatric cerebellar tumors. *Acad. Radiol.* **2012**, *19*, 794–800. [CrossRef]
98. Poussaint, T.Y.; Rodriguez, D. Advanced neuroimaging of pediatric brain tumors: MR diffusion, MR perfusion, and MR spectroscopy. *Neuroimaging Clin. N. Am.* **2006**, *16*, 169–192, ix. [CrossRef] [PubMed]
99. Rodallec, M.; Colombat, M.; Krainik, A.; Kalamaridès, M.; Redondo, A.; Feydy, A. Diffusion-weighted MR imaging and pathologic findings in adult cerebellar medulloblastoma. *J. Neuroradiol.* **2004**, *31*, 234–237. [CrossRef] [PubMed]
100. Quadery, F.A.; Okamoto, K. Diffusion-weighted MRI of haemangioblastomas and other cerebellar tumours. *Neuroradiology* **2003**, *45*, 212–219. [CrossRef] [PubMed]
101. Wilke, M.; Eidenschink, A.; Müller-Weihrich, S.; Auer, D.P. MR diffusion imaging and 1H spectroscopy in a child with medulloblastoma. A case report. *Acta Radiol.* **2001**, *42*, 39–42. [PubMed]
102. Kotsenas, A.L.; Roth, T.C.; Manness, W.K.; Faerber, E.N. Abnormal diffusion-weighted MRI in medulloblastoma: Does it reflect small cell histology? *Pediatr. Radiol.* **1999**, *29*, 524–526. [CrossRef] [PubMed]
103. Zitouni, S.; Koc, G.; Doganay, S.; Saracoglu, S.; Gumus, K.Z.; Ciraci, S.; Coskun, A.; Unal, E.; Per, H.; Kurtsoy, A.; et al. Apparent diffusion coefficient in differentiation of pediatric posterior fossa tumors. *Jpn. J. Radiol.* **2017**, *35*, 448–453. [CrossRef] [PubMed]
104. Pillai, S.; Singhal, A.; Byrne, A.T.; Dunham, C.; Cochrane, D.D.; Steinbok, P. Diffusion-weighted imaging and pathological correlation in pediatric medulloblastomas-"They are not always restricted!". *Childs Nerv. Syst.* **2011**, *27*, 1407–1411. [CrossRef]
105. Douglas-Akinwande, A.C.; Payner, T.D.; Hattab, E.M. Medulloblastoma mimicking Lhermitte-Duclos disease on MRI and CT. *Clin. Neurol. Neurosurg.* **2009**, *111*, 536–539. [CrossRef] [PubMed]
106. Jaremko, J.L.; Jans, L.B.; Coleman, L.T.; Ditchfield, M.R. Value and limitations of diffusion-weighted imaging in grading and diagnosis of pediatric posterior fossa tumors. *AJNR Am. J. Neuroradiol.* **2010**, *31*, 1613–1616. [CrossRef]
107. Forbes, J.A.; Reig, A.S.; Smith, J.G.; Jermakowicz, W.; Tomycz, L.; Shay, S.D.; Sun, D.A.; Wushensky, C.A.; Pearson, M.M. Findings on preoperative brain MRI predict histopathology in children with cerebellar neoplasms. *Pediatr. Neurosurg.* **2011**, *47*, 51–59. [CrossRef]
108. Orman, G.; Bosemani, T.; Higgins, L.; Carson, K.A.; Huisman, T.A.; Poretti, A. Pediatric Cerebellar Tumors: Does ADC Analysis of Solid, Contrast-Enhancing Tumor Components Correlate Better with Tumor Grade than ADC Analysis of the Entire Tumor? *J. Neuroimaging* **2015**, *25*, 785–791. [CrossRef]
109. Porto, L.; Jurcoane, A.; Schwabe, D.; Kieslich, M.; Hattingen, E. Differentiation between high and low grade tumours in paediatric patients by using apparent diffusion coefficients. *Eur. J. Paediatr. Neurol.* **2013**, *17*, 302–307. [CrossRef] [PubMed]
110. Pierce, T.; Kranz, P.G.; Roth, C.; Leong, D.; Wei, P.; Provenzale, J.M. Use of apparent diffusion coefficient values for diagnosis of pediatric posterior fossa tumors. *Neuroradiol. J.* **2014**, *27*, 233–244. [CrossRef]
111. Pierce, T.T.; Provenzale, J.M. Evaluation of apparent diffusion coefficient thresholds for diagnosis of medulloblastoma using diffusion-weighted imaging. *Neuroradiol. J.* **2014**, *27*, 63–74. [CrossRef] [PubMed]
112. Koral, K.; Mathis, D.; Gimi, B.; Gargan, L.; Weprin, B.; Bowers, D.C.; Margraf, L. Common pediatric cerebellar tumors: Correlation between cell densities and apparent diffusion coefficient metrics. *Radiology* **2013**, *268*, 532–537. [CrossRef] [PubMed]
113. Koral, K.; Alford, R.; Choudhury, N.; Mossa-Basha, M.; Gargan, L.; Gimi, B.; Gao, A.; Zhang, S.; Bowers, D.C.; Koral, K.M.; et al. Applicability of apparent diffusion coefficient ratios in preoperative diagnosis of common pediatric cerebellar tumors across two institutions. *Neuroradiology* **2014**, *56*, 781–788. [CrossRef] [PubMed]
114. Domínguez-Pinilla, N.; Martínez de Aragón, A.; Diéguez Tapias, S.; Toldos, O.; Hinojosa Bernal, J.; Rigal Andrés, M.; González-Granado, L.I. Evaluating the apparent diffusion coefficient in MRI studies as a means of determining paediatric brain tumour stages. *Neurologia* **2016**, *31*, 459–465. [CrossRef]
115. Wagner, M.W.; Narayan, A.K.; Bosemani, T.; Huisman, T.A.; Poretti, A. Histogram Analysis of Diffusion Tensor Imaging Parameters in Pediatric Cerebellar Tumors. *J. Neuroimaging* **2016**, *26*, 360–365. [CrossRef] [PubMed]
116. Assis, Z.A.; Saini, J.; Ranjan, M.; Gupta, A.K.; Sabharwal, P.; Naidu, P.R. Diffusion tensor imaging in evaluation of posterior fossa tumors in children on a 3T MRI scanner. *Indian J. Radiol. Imaging* **2015**, *25*, 445–452. [CrossRef]
117. Dangouloff-Ros, V.; Varlet, P.; Levy, R.; Beccaria, K.; Puget, S.; Dufour, C.; Boddaert, N. Imaging features of medulloblastoma: Conventional imaging, diffusion-weighted imaging, perfusion-weighted imaging, and spectroscopy: From general features to subtypes and characteristics. *Neurochirurgie* **2021**, *67*, 6–13. [CrossRef]
118. Gauvain, K.M.; McKinstry, R.C.; Mukherjee, P.; Perry, A.; Neil, J.J.; Kaufman, B.A.; Hayashi, R.J. Evaluating pediatric brain tumor cellularity with diffusion-tensor imaging. *AJR Am. J. Roentgenol.* **2001**, *177*, 449–454. [CrossRef]
119. Burger, P.C.; Yu, I.T.; Tihan, T.; Friedman, H.S.; Strother, D.R.; Kepner, J.L.; Duffner, P.K.; Kun, L.E.; Perlman, E.J. Atypical teratoid/rhabdoid tumor of the central nervous system: A highly malignant tumor of infancy and childhood frequently mistaken for medulloblastoma: A Pediatric Oncology Group study. *Am. J. Surg. Pathol.* **1998**, *22*, 1083–1092. [CrossRef]
120. Phuttharak, W.; Wannasarnmetha, M.; Wara-Asawapati, S.; Yuthawong, S. Diffusion MRI in Evaluation of Pediatric Posterior Fossa Tumors. *Asian Pac. J. Cancer Prev.* **2021**, *22*, 1129–1136. [CrossRef]
121. Filippi, C.G.; Edgar, M.A.; Uluğ, A.M.; Prowda, J.C.; Heier, L.A.; Zimmerman, R.D. Appearance of meningiomas on diffusion-weighted images: Correlating diffusion constants with histopathologic findings. *AJNR Am. J. Neuroradiol.* **2001**, *22*, 65–72. [PubMed]
122. Toh, C.H.; Castillo, M.; Wong, A.M.; Wei, K.C.; Wong, H.F.; Ng, S.H.; Wan, Y.L. Differentiation between classic and atypical meningiomas with use of diffusion tensor imaging. *AJNR Am. J. Neuroradiol.* **2008**, *29*, 1630–1635. [CrossRef] [PubMed]

123. Tamrazi, B.; Shiroishi, M.S.; Liu, C.S. Advanced Imaging of Intracranial Meningiomas. *Neurosurg. Clin. N. Am.* **2016**, *27*, 137–143. [CrossRef] [PubMed]

124. Babu, S.; Uppin, S.G.; Uppin, M.S.; Panigrahi, M.K.; Saradhi, V.; Bhattacharjee, S.; Sahu, B.P.; Purohit, A.K.; Challa, S. Meningiomas: Correlation of Ki67 with histological grade. *Neurol. India* **2011**, *59*, 204–207. [CrossRef] [PubMed]

125. Abry, E.; Thomassen, I.Ø.; Salvesen, Ø.O.; Torp, S.H. The significance of Ki-67/MIB-1 labeling index in human meningiomas: A literature study. *Pathol. Res. Pract.* **2010**, *206*, 810–815. [CrossRef] [PubMed]

126. Padhani, A.R.; Liu, G.; Koh, D.M.; Chenevert, T.L.; Thoeny, H.C.; Takahara, T.; Dzik-Jurasz, A.; Ross, B.D.; Van Cauteren, M.; Collins, D.; et al. Diffusion-weighted magnetic resonance imaging as a cancer biomarker: Consensus and recommendations. *Neoplasia* **2009**, *11*, 102–125. [CrossRef] [PubMed]

127. Tsai, Y.T.; Hung, K.C.; Shih, Y.J.; Lim, S.W.; Yang, C.C.; Kuo, Y.T.; Chen, J.H.; Ko, C.C. Preoperative Apparent Diffusion Coefficient Values for Differentiation between Low and High Grade Meningiomas: An Updated Systematic Review and Meta-Analysis. *Diagnostics* **2022**, *12*, 630. [CrossRef]

128. Meyer, H.J.; Wienke, A.; Surov, A. ADC values of benign and high grade meningiomas and associations with tumor cellularity and proliferation—A systematic review and meta-analysis. *J. Neurol. Sci.* **2020**, *415*, 116975. [CrossRef]

129. Watanabe, K.; Kakeda, S.; Yamamoto, J.; Ide, S.; Ohnari, N.; Nishizawa, S.; Korogi, Y. Prediction of hard meningiomas: Quantitative evaluation based on the magnetic resonance signal intensity. *Acta Radiol.* **2016**, *57*, 333–340. [CrossRef] [PubMed]

130. Hoover, J.M.; Morris, J.M.; Meyer, F.B. Use of preoperative magnetic resonance imaging T1 and T2 sequences to determine intraoperative meningioma consistency. *Surg. Neurol. Int.* **2011**, *2*, 142. [CrossRef]

131. Yogi, A.; Koga, T.; Azama, K.; Higa, D.; Ogawa, K.; Watanabe, T.; Ishiuchi, S.; Murayama, S. Usefulness of the apparent diffusion coefficient (ADC) for predicting the consistency of intracranial meningiomas. *Clin. Imaging* **2014**, *38*, 802–807. [CrossRef] [PubMed]

132. Kashimura, H.; Inoue, T.; Ogasawara, K.; Arai, H.; Otawara, Y.; Kanbara, Y.; Ogawa, A. Prediction of meningioma consistency using fractional anisotropy value measured by magnetic resonance imaging. *J. Neurosurg.* **2007**, *107*, 784–787. [CrossRef] [PubMed]

133. Shiroishi, M.S.; Cen, S.Y.; Tamrazi, B.; D'Amore, F.; Lerner, A.; King, K.S.; Kim, P.E.; Law, M.; Hwang, D.H.; Boyko, O.B.; et al. Predicting Meningioma Consistency on Preoperative Neuroimaging Studies. *Neurosurg. Clin. N. Am.* **2016**, *27*, 145–154. [CrossRef] [PubMed]

134. Sinha, S.; Sharma, B.S. Cystic acoustic neuromas: Surgical outcome in a series of 58 patients. *J. Clin. Neurosci.* **2008**, *15*, 511–515. [CrossRef]

135. Sawamura, Y.; Shirato, H.; Sakamoto, T.; Aoyama, H.; Suzuki, K.; Onimaru, R.; Isu, T.; Fukuda, S.; Miyasaka, K. Management of vestibular schwannoma by fractionated stereotactic radiotherapy and associated cerebrospinal fluid malabsorption. *J. Neurosurg.* **2003**, *99*, 685–692. [CrossRef] [PubMed]

136. Myrseth, E.; Møller, P.; Pedersen, P.H.; Lund-Johansen, M. Vestibular schwannoma: Surgery or gamma knife radiosurgery? A prospective, nonrandomized study. *Neurosurgery* **2009**, *64*, 654–661; Discussion, 661–663. [CrossRef]

137. Lin, Y.C.; Wang, C.C.; Wai, Y.Y.; Wan, Y.L.; Ng, S.H.; Chen, Y.L.; Liu, H.L.; Wang, J.J. Significant temporal evolution of diffusion anisotropy for evaluating early response to radiosurgery in patients with vestibular schwannoma: Findings from functional diffusion maps. *AJNR Am. J. Neuroradiol.* **2010**, *31*, 269–274. [CrossRef]

138. Camargo, A.; Schneider, T.; Liu, L.; Pakpoor, J.; Kleinberg, L.; Yousem, D.M. Pretreatment ADC Values Predict Response to Radiosurgery in Vestibular Schwannomas. *AJNR Am. J. Neuroradiol.* **2017**, *38*, 1200–1205. [CrossRef]

139. Barajas, R.F., Jr.; Cha, S. Metastasis in Adult Brain Tumors. *Neuroimaging Clin. N. Am.* **2016**, *26*, 601–620. [CrossRef]

140. Svokos, K.A.; Salhia, B.; Toms, S.A. Molecular biology of brain metastasis. *Int. J. Mol. Sci.* **2014**, *15*, 9519–9530. [CrossRef]

141. Ulu, E.; Ozturk, B.; Atalay, K.; Okumus, I.B.; Erdem, D.; Gul, M.K.; Terzi, O. Diffusion-Weighted Imaging of Brain Metastasis: Correlation of MRI Parameters with Histologic Type. *Turk. Neurosurg.* **2022**, *32*, 58–68. [CrossRef] [PubMed]

142. Duygulu, G.; Ovali, G.Y.; Calli, C.; Kitis, O.; Yünten, N.; Akalin, T.; Islekel, S. Intracerebral metastasis showing restricted diffusion: Correlation with histopathologic findings. *Eur. J. Radiol.* **2010**, *74*, 117–120. [CrossRef] [PubMed]

143. Hayashida, Y.; Hirai, T.; Morishita, S.; Kitajima, M.; Murakami, R.; Korogi, Y.; Makino, K.; Nakamura, H.; Ikushima, I.; Yamura, M.; et al. Diffusion-weighted imaging of metastatic brain tumors: Comparison with histologic type and tumor cellularity. *AJNR Am. J. Neuroradiol.* **2006**, *27*, 1419–1425. [PubMed]

144. Koyama, H.; Ohno, Y.; Nishio, M.; Takenaka, D.; Yoshikawa, T.; Matsumoto, S.; Seki, S.; Maniwa, Y.; Ito, T.; Nishimura, Y.; et al. Diffusion-weighted imaging vs. STIR turbo SE imaging: Capability for quantitative differentiation of small-cell lung cancer from non-small-cell lung cancer. *Br. J. Radiol.* **2014**, *87*, 20130307. [CrossRef] [PubMed]

145. Liu, H.; Liu, Y.; Yu, T.; Ye, N. Usefulness of diffusion-weighted MR imaging in the evaluation of pulmonary lesions. *Eur. Radiol.* **2010**, *20*, 807–815. [CrossRef]

146. Meyer, H.J.; Fiedler, E.; Kornhuber, M.; Spielmann, R.P.; Surov, A. Comparison of diffusion-weighted imaging findings in brain metastases of different origin. *Clin. Imaging* **2015**, *39*, 965–969. [CrossRef]

147. Zakaria, R.; Das, K.; Radon, M.; Bhojak, M.; Rudland, P.R.; Sluming, V.; Jenkinson, M.D. Diffusion-weighted MRI characteristics of the cerebral metastasis to brain boundary predicts patient outcomes. *BMC Med. Imaging* **2014**, *14*, 26. [CrossRef]

148. Jung, W.S.; Park, C.H.; Hong, C.K.; Suh, S.H.; Ahn, S.J. Diffusion-Weighted Imaging of Brain Metastasis from Lung Cancer: Correlation of MRI Parameters with the Histologic Type and Gene Mutation Status. *AJNR Am. J. Neuroradiol.* **2018**, *39*, 273–279. [CrossRef]

149. Mahendru, G.; Chong, V. Meninges in cancer imaging. *Cancer Imaging* **2009**, *9*, S14–S21. [CrossRef]

150. Bulakbasi, N.; Guvenc, I.; Onguru, O.; Erdogan, E.; Tayfun, C.; Ucoz, T. The added value of the apparent diffusion coefficient calculation to magnetic resonance imaging in the differentiation and grading of malignant brain tumors. *J. Comput. Assist. Tomogr.* **2004**, *28*, 735–746. [CrossRef]

151. Pope, W.B. Brain metastases: Neuroimaging. *Handb. Clin. Neurol.* **2018**, *149*, 89–112. [CrossRef] [PubMed]

152. Romano, A.; Moltoni, G.; Guarnera, A.; Pasquini, L.; Di Napoli, A.; Napolitano, A.; Espagnet, M.C.R.; Bozzao, A. Single brain metastasis versus glioblastoma multiforme: A VOI-based multiparametric analysis for differential diagnosis. *Radiol. Med.* **2022**, *127*, 490–497. [CrossRef] [PubMed]

153. Pavlisa, G.; Rados, M.; Pavlisa, G.; Pavic, L.; Potocki, K.; Mayer, D. The differences of water diffusion between brain tissue infiltrated by tumor and peritumoral vasogenic edema. *Clin. Imaging* **2009**, *33*, 96–101. [CrossRef] [PubMed]

154. Han, C.; Huang, S.; Guo, J.; Zhuang, X.; Han, H. Use of a high b-value for diffusion weighted imaging of peritumoral regions to differentiate high-grade gliomas and solitary metastases. *J. Magn. Reson. Imaging* **2015**, *42*, 80–86. [CrossRef] [PubMed]

155. Miquelini, L.A.; Pérez Akly, M.S.; Funes, J.A.; Besada, C.H. Usefulness of the apparent diffusion coefficient for the evaluation of the white matter to differentiate between glioblastoma and brain metastases. *Radiologia* **2016**, *58*, 207–213. [CrossRef] [PubMed]

156. Kalpathy-Cramer, J.; Gerstner, E.R.; Emblem, K.E.; Andronesi, O.; Rosen, B. Advanced magnetic resonance imaging of the physical processes in human glioblastoma. *Cancer Res.* **2014**, *74*, 4622–4637. [CrossRef] [PubMed]

157. Pirzkall, A.; McGue, C.; Saraswathy, S.; Cha, S.; Liu, R.; Vandenberg, S.; Lamborn, K.R.; Berger, M.S.; Chang, S.M.; Nelson, S.J. Tumor regrowth between surgery and initiation of adjuvant therapy in patients with newly diagnosed glioblastoma. *Neuro-Oncology* **2009**, *11*, 842–852. [CrossRef]

158. Oberheim Bush, N.A.; Hervey-Jumper, S.L.; Berger, M.S. Management of Glioblastoma, Present and Future. *World Neurosurg.* **2019**, *131*, 328–338. [CrossRef] [PubMed]

159. Matsushita, T.; Anami, D.; Arioka, T.; Inoue, S.; Kariya, Y.; Fujimoto, M.; Ida, K.; Sasai, N.; Kaji, M.; Kanazawa, S.; et al. Basic study of susceptibility-weighted imaging at 1.5T. *Acta Med. Okayama* **2008**, *62*, 159–168. [CrossRef]

160. Li, H.; Duan, Y.; Liu, N.; Dong, J.; Liang, Y.; Ju, R. Value of DWI Combined with Magnetic Resonance Spectroscopy in the Differential Diagnosis between Recurrent Glioma and Radiation Injury: A Meta-Analysis. *Int. J. Clin. Pract.* **2022**, *2022*, 1629570. [CrossRef]

161. Hegi, M.E.; Liu, L.; Herman, J.G.; Stupp, R.; Wick, W.; Weller, M.; Mehta, M.P.; Gilbert, M.R. Correlation of O6-methylguanine methyltransferase (MGMT) promoter methylation with clinical outcomes in glioblastoma and clinical strategies to modulate MGMT activity. *J. Clin. Oncol.* **2008**, *26*, 4189–4199. [CrossRef] [PubMed]

162. Kondo, M.; Uchiyama, Y. Apparent diffusion coefficient histogram analysis for prediction of prognosis in glioblastoma. *J. Neuroradiol.* **2018**, *45*, 236–241. [CrossRef] [PubMed]

163. Barajas, R.F., Jr.; Phillips, J.J.; Parvataneni, R.; Molinaro, A.; Essock-Burns, E.; Bourne, G.; Parsa, A.T.; Aghi, M.K.; McDermott, M.W.; Berger, M.S.; et al. Regional variation in histopathologic features of tumor specimens from treatment-naive glioblastoma correlates with anatomic and physiologic MR Imaging. *Neuro-Oncology* **2012**, *14*, 942–954. [CrossRef] [PubMed]

164. Chang, E.L.; Akyurek, S.; Avalos, T.; Rebueno, N.; Spicer, C.; Garcia, J.; Famiglietti, R.; Allen, P.K.; Chao, K.S.; Mahajan, A.; et al. Evaluation of peritumoral edema in the delineation of radiotherapy clinical target volumes for glioblastoma. *Int. J. Radiat. Oncol. Biol. Phys.* **2007**, *68*, 144–150. [CrossRef]

165. Rathore, S.; Akbari, H.; Doshi, J.; Shukla, G.; Rozycki, M.; Bilello, M.; Lustig, R.; Davatzikos, C. Radiomic signature of infiltration in peritumoral edema predicts subsequent recurrence in glioblastoma: Implications for personalized radiotherapy planning. *J. Med. Imaging* **2018**, *5*, 021219. [CrossRef]

166. Pasquini, L.; Di Napoli, A.; Napolitano, A.; Lucignani, M.; Dellepiane, F.; Vidiri, A.; Villani, V.; Romano, A.; Bozzao, A. Glioblastoma radiomics to predict survival: Diffusion characteristics of surrounding nonenhancing tissue to select patients for extensive resection. *J. Neuroimaging* **2021**, *31*, 1192–1200. [CrossRef]

167. Fathalla, H.; Cusimano, M.D.; Di Ieva, A.; Lee, J.; Alsharif, O.; Goguen, J.; Zhang, S.; Smyth, H. Endoscopic versus microscopic approach for surgical treatment of acromegaly. *Neurosurg. Rev.* **2015**, *38*, 541–548; Discussion, 548–549. [CrossRef] [PubMed]

168. Abe, T.; Iwata, T.; Kawamura, N.; Izumiyama, H.; Ikeda, H.; Matsumoto, K. Staged transsphenoidal surgery for fibrous nonfunctioning pituitary adenomas with suprasellar extension. *Neurol. Med. Chir.* **1997**, *37*, 830–835; Discussion, 835–837. [CrossRef]

169. Mohamed, F.F.; Safwat, A. Diagnostic value of apparent diffusion coefficient (ADC) in assessment of pituitary macroadenoma consistency. *Egypt. J. Radiol. Nucl. Med.* **2013**, *44*, 617–624. [CrossRef]

170. Pierallini, A.; Caramia, F.; Falcone, C.; Tinelli, E.; Paonessa, A.; Ciddio, A.B.; Fiorelli, M.; Bianco, F.; Natalizi, S.; Ferrante, L.; et al. Pituitary macroadenomas: Preoperative evaluation of consistency with diffusion-weighted MR imaging—Initial experience. *Radiology* **2006**, *239*, 223–231. [CrossRef]

171. Suzuki, C.; Maeda, M.; Hori, K.; Kozuka, Y.; Sakuma, H.; Taki, W.; Takeda, K. Apparent diffusion coefficient of pituitary macroadenoma evaluated with line-scan diffusion-weighted imaging. *J. Neuroradiol.* **2007**, *34*, 228–235. [CrossRef] [PubMed]

172. Rutland, J.W.; Loewenstern, J.; Ranti, D.; Tsankova, N.M.; Bellaire, C.P.; Bederson, J.B.; Delman, B.N.; Shrivastava, R.K.; Balchandani, P. Analysis of 7-tesla diffusion-weighted imaging in the prediction of pituitary macroadenoma consistency. *J. Neurosurg.* **2020**, *134*, 771–779. [CrossRef] [PubMed]

173. Ding, W.; Huang, Z.; Zhou, G.; Li, L.; Zhang, M.; Li, Z. Diffusion-weighted imaging for predicting tumor consistency and extent of resection in patients with pituitary adenoma. *Neurosurg. Rev.* **2021**, *44*, 2933–2941. [CrossRef] [PubMed]

174. Sanei Taheri, M.; Kimia, F.; Mehrnahad, M.; Saligheh Rad, H.; Haghighatkhah, H.; Moradi, A.; Kazerooni, A.F.; Alviri, M.; Absalan, A. Accuracy of diffusion-weighted imaging-magnetic resonance in differentiating functional from non-functional pituitary macro-adenoma and classification of tumor consistency. *Neuroradiol. J.* **2019**, *32*, 74–85. [CrossRef] [PubMed]

175. Doai, M.; Tonami, H.; Matoba, M.; Tachibana, O.; Iizuka, H.; Nakada, S.; Yamada, S. Pituitary macroadenoma: Accuracy of apparent diffusion coefficient magnetic resonance imaging in grading tumor aggressiveness. *Neuroradiol. J.* **2019**, *32*, 86–91. [CrossRef]

176. Gomez, C.K.; Schiffman, S.R.; Bhatt, A.A. Radiological review of skull lesions. *Insights Imaging* **2018**, *9*, 857–882. [CrossRef]

177. Tu, Z.; Xiao, Z.; Zheng, Y.; Huang, H.; Yang, L.; Cao, D. Benign and malignant skull-involved lesions: Discriminative value of conventional CT and MRI combined with diffusion-weighted MRI. *Acta Radiol.* **2019**, *60*, 880–886. [CrossRef]

178. Soni, N.; Gupta, N.; Kumar, Y.; Mangla, M.; Mangla, R. Role of diffusion-weighted imaging in skull base lesions: A pictorial review. *Neuroradiol. J.* **2017**, *30*, 370–384. [CrossRef]

179. Mahendrakar, A.K.; Kumaran, S.P.; Reddy, B.N.; Viswamitra, S. Utility of apparent diffusion coefficient (ADC) values in differentiating benign and malignant skull lesions with histopathological (HPE) correlation. *J. Clin. Neurosci.* **2022**, *98*, 21–28. [CrossRef]